Z. Phys. C – Particles and Fields 53, 617–628 (1992)

Zeitschrift für Physik C Particles and Fields
© Springer-Verlag 1992

On estimating the top quark mass from global analyses of e^+e^- collision data

D. Levinthal,[1] F. Bird[2,a], R.G. Stuart[2], B.W. Lynn[3]

[1] Florida State University, Tallahassee, FL 32306-3016, USA
[2] CERN, CH-1211 Geneva 23, Switzerland
[3] Stanford University, Stanford, CA 94305, USA

Received 15 June 1991; in revised form 6 September 1991

Abstract. A study is undertaken to determine how to best extract the top quark mass m_t within the Minimal Standard Model (MSM) using a global fit to a variety of processes (including wide-angle Bhabha scattering) in e^+e^- collisions near the Z which should be measured in the coming years. Experimental cuts are accommodated as an integral part of the analysis. It is advantageous to use the collinear radiation approximation and to cut data in rapidity, center-of-mass polar angle and minimum final state invariant mass squared, s'. This avoids the need for the largest Monte Carlo acceptance correction to the data. Further, high precision cross section calculations (which include all one-loop electroweak and QED effects, certain higher-order improvements and perturbative QCD corrections as well as exponentiated soft and collinear photon radiation) then no longer require a Monte Carlo. This results in a speedup factor of at least fifty thousand ($>5\times10^4$) in EXPOSTAR. The data (corrected only for detector cracks, resolution and small non-collinear radiation effects) can therefore be fit quickly and directly for M_Z, m_t, m_{Higgs} and α_{strong} without recourse to unphysical intermediate quantities (weak mixing angles, running couplings, partial widths, κ*, etc.). Determination of m_t could be as precise as ±15 GeV (and another ±20 GeV from m_{Higgs}) at the end of LEP running in 1991. Longitudinally polarized beams with very small polarization error could give an error on m_t smaller by a factor ≈4 for the same luminosity.

1 Introduction

With the basic confirmation of the $SU(2)\times U(1)$ electroweak model as determined by measurements of the intermediate vector bosons at LEP and the proton-antiproton colliders, the underlying gauge structure of the theory is now being studied through the higher order virtual contributions to the observable cross sections. Improvements in the accuracy of the studies will be made by including measurements from many distinct Z decay processes in a global analysis. Such a global analysis will become the standard method for analyzing the data. In order to determine the optimal strategy for making these studies, many different observables should be calculated where all of the virtual contributions are computed within a single, consistent framework. In addition, the full and proper statistical treatment of the data samples needs to be incorporated into any model of a measurement strategy. To this end, EXPOSTAR [1, 2] has been modified [3] to be used in conjunction with a fitting program for direct comparisons of data to the Minimal Standard Model (MSM) of Glashow, Salam and Weinberg [4]. (The MSM is defined here to be electroweak $SU(2)\times U(1)$ with three families of quarks and leptons and one Higgs doublet.) In this form, the program can be used to fit real data, or as is done here, to calculate mock data samples, which can then be fit to determine the sensitivity of various combinations of data sets to the virtual effects of a heavy top quark.

Experimentally, cuts are required to achieve a well-measured data sample, since there are backgrounds and detector inefficiencies. By incorporating the cuts into the calculations, the reliance on Monte Carlo simulations is reduced. The typical LEP detector is very efficient for Z decays, limited by regions near the beam pipe and minimum energy requirements of the triggers. For hadronic final states, only the minimum energy requirement is important, since jet properties ensure that LEP detectors have high geometrical efficiency. The use of cuts in three orthogonal variables, the collision-frame scattering angle, the longitudinal rapidity of the final state, and the minimum invariant energy in the final state, produce an accepted phase space for leptonic final states which is only affected by resolution and detector cracks.

In order to investigate the compatibility of the MSM with the data, an appropriate scheme for cross section calculations must be developed. Such a novel scheme (for e^+e^- experiments) has been adopted here and will be discussed in the next section of this paper. Subsequently,

[a] Permanent address: S.S.C. Laboratory, Dallas, Texas, USA

applications of the technique will be discussed, followed by the mock data study for LEP-like event samples.

2 Collinear radiation and rapidity

As is well known, initial state radiative effects constitute large corrections (on the order of 30% at the Z resonance peak) to any cross section calculation which is to be compared to LEP data [5, 6]. To account for this, here, as within EXPOSTAR, the collinear radiation approximation [7] is used. This approximation is quite accurate at LEP energies where collinear radiation is enhanced via $\ln(s/m_e^2) \approx 24$, so that it is much larger than the hard non-collinear terms. This assumption allows the computation of a cross section as a convolution integral of two electron structure functions with invariant collision-frame cross sections evaluated at reduced energy [5, 6, 8, 9, 10]. The electron structure functions are the probability densities for the initial state leptons to have radiated away some fraction of the full beam energy. The center-of-mass cross sections can be evaluated in the rest-frame of the collision where the kinematics are simple. The techniques used here are familiar to analysts of hadronic experiments [11, 12], but are only partially used in the study of e^+e^- interactions [2, 8, 9, 10, 13].

With $s=(2E_b)^2$, the square of the center of mass energy, and x_- (x_+) the fraction of the beam energy (E_b) an initial state electron (positron) has after radiation ($0 \le x_\pm \le 1$), and $\cos\theta'$, the center-of-mass scattering angle, the differential cross section can be written as

$$\left.\frac{d\sigma}{d\cos\theta'}\right|_s = \left(\int dx_+\, dx_-\, D(x_+, s) D(x_-, s) \times \frac{d\sigma(s x_+ x_-, \cos\theta')}{d\cos\theta'} \right) + \square_{Z\gamma} + \square_{\gamma\gamma},$$

and the total cross section as

$$\sigma(s) = \int d\cos\theta' \frac{d\sigma}{d\cos\theta'},$$

where $d\sigma(s x_+ x_-, \cos\theta')/d\cos\theta'$ is the collision-frame differential cross section (containing electroweak loop and final state radiation corrections), the structure function $D(x_\pm, s)$ represents the probability of a beam particle having a fraction $x_\pm$ of its original energy after initial state radiation [8–10] and $\square_{Z\gamma}$ and $\square_{\gamma\gamma}$ are the contributions from the order α^3 sum of (photon-Z and 2-photon boxes) × Born and bremsstrahlung processes which are not absorbed in $D(x_\pm, s)$ or in the final state radiation factor.

Introducing the fractional reduced collision-frame invariant energy-squared $s' = \chi s$ where

$$\chi = x_+ x_-,$$

and the rapidity Y,

$$Y = \ln\sqrt{\frac{x_+}{x_-}},$$

gives the *factorized* radiation convolution integral

$$\left.\frac{d\sigma}{d\cos\theta'}\right|_s = \int d\chi \left(\frac{d\sigma(s\chi, \cos\theta')}{d\cos\theta'} H_s(\chi, s) \right) + \square_{Z\gamma} + \square_{\gamma\gamma},$$

where, when the integral extends to the kinematic limits ($Y = \pm \ln\sqrt{\chi}$), the flux factor

$$H_s(\chi, s) = \int dY D(\sqrt{\chi} e^{+Y}, s) D(\sqrt{\chi} e^{-Y}, s)$$

is equivalent to other formulations [8–10].

When a rapidity cut ($|Y| \le Y_{\max}$) is applied to the data, the flux factor cannot be taken from the literature directly, but a numerical integration over rapidity of the structure functions must be evaluated. The integral has the interesting property that for $\chi \ge e^{-2Y_{\max}}$ the range of integration is the whole of phase space. In that case the published flux factors can be used to improve numerical accuracy. In either case most of the non-collinear terms can also be absorbed [9]. The rapidity integration, when extended to the kinematic limit, has been shown to be numerically consistent with published formulae [9] to $<1\%$ in the hard radiation region where it must be used.

Because of the factorization of the radiation convolution integral, inclusion of the rapidity cut in the flux factor $H_s(\chi, s)$ eliminates (in the collinear radiation approximation) the need for the Monte Carlo in high precision electroweak calculations of differential distributions in $\cos\theta'$ for LEP processes. The result is a huge speedup factor in these calculations which, as will be shown, allows direct comparison of the electroweak theory (including quantum loop corrections) to LEP data (corrected only for resolution, detector cracks and small non-collinear radiation effects).

Extending the collinear radiation assumption to the final state implies that final state radiation leaves the directions of the final state fermions unchanged. We have defined s' as

$$s' = s\chi = 2p_+ p_- (1 - \cos(\theta_+ - \theta_-)) = 2p_t^2 \left(\frac{1 - \cos(\theta_+ - \theta_-)}{\sin\theta_+ \sin\theta_-} \right)$$

in the lab-frame with θ_- and θ_+ the electron and positron polar angles. In the collision-frame

$$s' = \frac{4p_t'^2}{\sin^2\theta'},$$

so that

$$\sin^2\theta' = \frac{2\sin\theta_+ \sin\theta_-}{1 - \cos(\theta_+ - \theta_-)}$$

is the ratio of the invariants (with respect to longitudinal boosts) $s\chi$ and p_t^2. Y, the longitudinal rapidity, is given by

$$Y = \ln\sqrt{\frac{E + p_z}{E - p_z}} = \ln\sqrt{\frac{\frac{1}{\sin\theta_+} + \frac{1}{\sin\theta_-} + \cot\theta_+ + \cot\theta_-}{\frac{1}{\sin\theta_+} + \frac{1}{\sin\theta_+} - \cot\theta_+ - \cot\theta_-}},$$

and is a function only of the lab polar angles of the final state leptons making it *accessible experimentally* in a simple manner.

It is in the discussion of the wide-angle Bhabha cross section that the utility of defining cross sections in the collision-frame becomes apparent. Momentum conservation at the vertex in the t-channel graphs mixes the initial and final states and usually prohibits the χ-Y factorization, the fundamental ansatz of this treatment, when the final state momenta are fixed. However, here the differential cross sections are being evaluated at fixed collision-frame angle, where the momentum transfer, q^2, is simply

$$-q^2 = t' = \frac{-s'}{2}(1-\cos\theta') = -\chi\frac{s(1-\cos\theta')}{2}.$$

This restores the factorized form of the simple calculation. While this is commonly done in calculations of high p_t hadron production to avoid the pole at $t'=0$, this is the first instance of this technique being applied to $e^+e^- \to e^+e^-$ scattering. The initial state photonic corrections must also be treated differently due to the t-channel. A large class of collinear and non-collinear corrections can be absorbed into the convolution integral if two flux factors are used. The s-channel amplitude is multiplied by the root of the flux factor used for the s-channel calculations. The t-channel amplitude is multiplied by a corresponding factor corrected for the different non-collinear terms [14], retaining only the leading logarithm for the α^4 correction [15], but evaluated at $q^2 = -t$. This procedure and the form of the t-channel flux factor are elaborated upon in Appendices A and B. The resulting cross term is also consistent with [14]. In this way there is no compromise made in the pure s-channel part of the calculation.

A rapidity cut constitutes an angle-dependent acollinearity cut, as seen in Fig. 1. In the collinear radiation approximation, such a cut leaves the $\cos\theta'$ distribution unaffected for s-channel processes.

A rapidity cut is more effective at eliminating $\gamma\gamma$ background than is an acollinearity cut since it is effective at all angles, while acollinearity cuts only remove backgrounds near 90°. A comparison is made in Fig. 2 of the efficiency as a function of the background-to-signal ratio for the two choices of cuts using the $\gamma\gamma$ Monte Carlo PHOT01 [16] and KORALZ [17] for muon events. For any value of background-to-signal, the rapidity cut is more efficient.

The effect on the phase space of such a rapidity cut can be calculated explicitly *without* recourse to a Monte Carlo. This means that a direct comparison of theory and data can be made without first having to simulate the effect of cuts on some Monte Carlo data sample. By making simultaneous cuts in $\cos\theta'$ and Y, the phase space corresponding to regions of low efficiency, e.g., the beam pipe region, can be excluded from the region of phase space used to measure cross sections altogether. For example, a detector with tracking coverage up to $\cos\theta_{\text{lab}} = 0.95$ loses less than 10^{-6} of $Z \to \mu^+\mu^-$ events, when $|\cos\theta'| < 0.90$ and $|Y| < 0.3$, due to this geometrical constraint. This is illustrated in Fig. 3, where the distribution of $\cos\theta_{\text{lab}}$ is shown for Bhabha events generated with BHABMC [18]. For the events in the plot, all have $|\cos\theta'| < 0.90$ and pass either a Y cut of 0.3 or an acollinearity cut of 25°. No tracks are observed beyond $|\cos\theta_{\text{lab}}| = 0.95$, the typical detector limit, when the Y cut is made. Thus, this combination of cuts produces, by itself, a precise phase space definition which minimizes the distortions of the true distributions. It is important to realize that it is the edges of the detector which limit the phase space of the measurement when an acollinearity cut is used, not the cuts themselves.

The non-collinear final state radiation [19] causes a small discrepancy (0.5% in the worst $\cos\theta'$ bin of the differential cross section) between the phase space defined by the experimental Y cut (defined with lepton polar angles only) and the true collision-frame rapidity cut used in the calculations. A small correction must be estimated by Monte Carlo to correct for this, a correction which is explicitly added into the χ^2 during fits to real data.

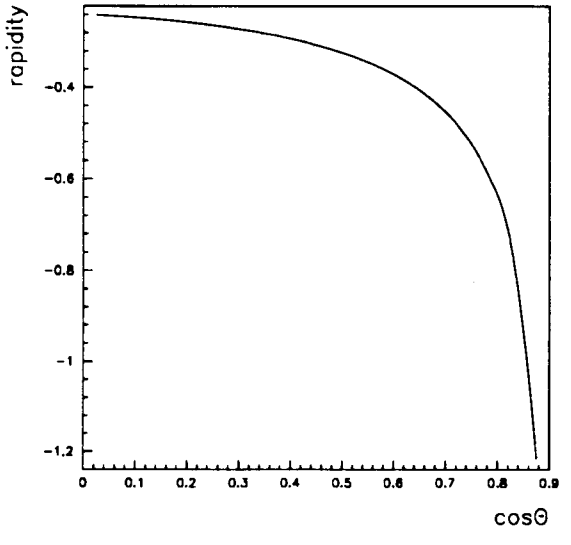

Fig. 1. Rapidity vs. $\cos\theta_{\text{lab}}$ for fixed 25° acollinearity

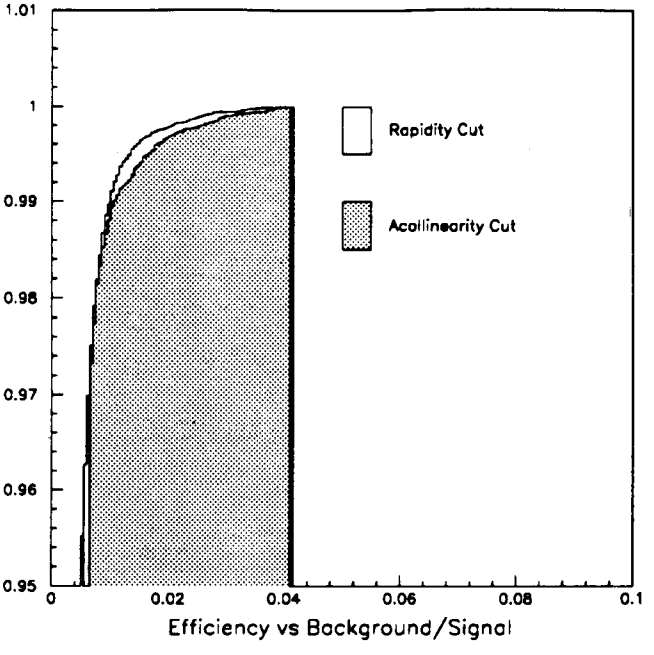

Fig. 2. Efficiency vs. background/signal

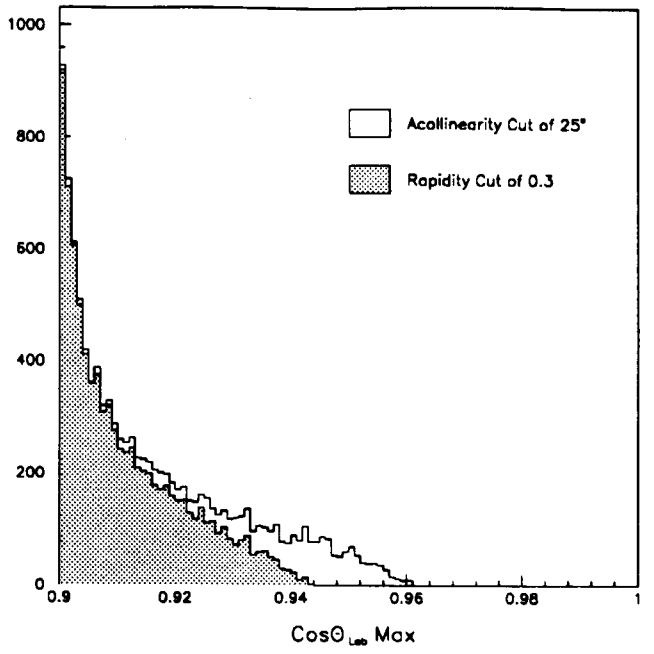

Fig. 3. $\cos\theta_{\text{lab}}$ distribution

A final cut on $\chi_{\min}=s'_{\min}/s$ can be accommodated where $\chi_{\min}$ is the minimum requirement on the square of the observed visible mass (final state radiation is included) and is the lower limit of the χ integration. This cut ensures that detailed knowledge of the extreme tail of the radiator functions is not necessary. This procedure is usually applied when measuring hadronic cross sections at LEP since there are uncertainties in the Monte Carlos when s' approaches quark mass thresholds. Measured leptonic cross sections are usually extrapolated to production threshold, a procedure which unnecessarily gives rise to a systematic error due to uncertainties in the Monte Carlo radiator functions at small s'. As long as this cut is at a small value ($\chi<0.1$) the calculation is insensitive to it to the level of typical experimental accuracies (0.2%), provided it is large enough to exclude the region where the divergent photon exchange term dominates, ($\chi>0.005$). These limits correspond to visible mass cuts between 6 and 29 GeV at the Z, as $\chi\approx(E_{\text{visible}}/2E_{\text{beam}})^2$.

Let us summarize the merits of rapidity, collision-frame angle and final invariant s' cuts over acollinearity, lab angle and extrapolation to fermion production threshold. In the collinear radiation approximation, a typical LEP experimental detector sees a region bounded in the χ-Y plane by the two exponentials defining the kinematic limit, a lower limit $\chi_{\min}^{\text{trigger}}$ defined by the trigger requirements, and a rapidity limit defined by the beam pipe region. As illustrated in Fig. 1, a fixed acollinearity cut corresponds, for a given lab angle, to a set of asymmetric rapidity cuts. The extrapolation by Monte Carlo to the fermion mass production threshold (typically well below $\chi_{\min}^{\text{trigger}}$) and kinematic rapidity limits is typically a 1% correction (a large effect for our purposes) and may be a source of unnecessary error. In principle a different Monte Carlo extrapolation is required for *each* angle in the construction of differential cross sections. In addition, there is a sociological complication, physicists outside the experimental collaborations have limited access to the details of these worrisome 'acceptance corrections' to the data, especially many years after the experimental collaborations have disbanded. This makes it very difficult for the physics community at large to make precise comparisons of LEP data to theory in the light of further electroweak developments. In contrast, experimental use of rapidity, collision frame angle and $\chi_{\min}$ cuts removes the need for these Monte Carlo extrapolations. An important feature is that the accepted data sample corresponds exactly to the phase space of any high precision electroweak calculation with a collinear radiation approximation (e.g. EXPOSTAR) without recourse to Monte Carlo. High precision electroweak calculations including the effects of cuts can then be done quickly and the data can be fit directly for *fundamental* electroweak parameters. Experimental differential cross sections published with this format would allow the entire physics community direct access to high precision electroweak experimental data.

3 Mock data fits

As input, EXPOSTAR is supplied with the experimentally well-measured parameters, $\alpha_{\text{QED}}(0)$ (the Thomson limit) and G_{Fermi} as determined from the muon lifetime. In addition the fit parameters the Z mass (M_Z), the Higgs mass (m_{Higgs}) and the top quark mass (m_t) are given. All three should be regarded as bookkeeping devices or external turning knobs which correspond, to some limited accuracy, to the physical values. It was recently emphasized [20, 21] that the on-shell definition of the Z^0 mass, currently extracted from LEP experiments, is significantly different from the usual one for the physical mass of an unstable particle based on the position of the pole of the matrix element on the complex s-plane. EXPOSTAR uses the input parameters to calculate the position of the pole from which the physical mass and total width can be easily extracted from the real and imaginary parts respectively. At the present time, m_t and m_{Higgs} may be identified with the physical parameters. The number of colors, N_C, may also be fit in order to vary the QCD final state corrections. These four parameters can be quickly and directly fit to the data (corrected only for detector cracks, resolution and small non-collinear radiation effects) without recourse to unphysical intermediate quantities (s_*^2, $\bar{s}^2$, $s^2_{\overline{MS}}$, effective running (* or other) couplings, partial widths, approximate Breit-Wigner widths, κ^*, effective vector/axial vector couplings, etc.); the EXPOSTAR user has no need to remember baroque definitions.

The collision-frame cross sections are constructed using the 'star' (*) scheme [1, 2] by absorbing most of the electroweak radiative corrections into running couplings [1, 22, 23] in an 'improved Born approximation'. The four effective q^2-dependent running couplings, e_*^2, s_*^2, G_μ^* and ρ_* are used primarily as a classification scheme for vector-boson self-energy loops (with certain 'non-abelian' parts of vertex and heavy box parts added for gauge invariance [1, 23–25]) and as a numerical bookkeeping device which

ensures self-consistency in the calculation of all electroweak s and t channel processes. The running couplings automatically resum [1] one-loop vector self-energies to all powers and so, when one-particle irreducible two-loop top-mass contributions to $\Delta_\rho(0)$ [26] are included, contain all important heavy top effects in the ρ parameter [27]. The leading $m_t^2 \alpha_{\text{strong}}$ effects are also included [28]. A dispersion relation is used to evaluate the light hadron contributions to vector self-energies [29]. Finally the residual vertex and box parts with internal heavy gauge bosons are added to the helicity amplitudes. These can be evaluated internally in either the s or t channel thus unifying the treatment of Bhabha scattering electroweak loops with that of pure s channel processes [1, 6, 30]. For b quark final states, large m_t effects are added in weak vertex parts [31, 32]. Of course, the b quark mass reduces the available final state phase space in both cross sections and the partial Z width to b's. For the final state, QED radiation factors are included for charged fermions as well as factorized perturbative QGD corrections for quarks.

Provision is made in EXPOSTAR for fitting LEP data directly with the contributions to vector self energies [30] of hypothesized $SU(2) \times U(1)$ heavy physics beyond MSM (more families of quarks and leptons [30], supersymmetry [30, 33] technicolor [30, 34], etc.) in the 3 parameters $\Delta'_3 = \Delta_3/q^2$, $\Delta'_+ = \Delta_+/q^2$ and $\Delta_\rho(0)$ as first discussed in [1]. This classification scheme for new physics has recently been popularized by many authors, all of whose three-parameter sets are equal to these up to overall constants [35]. In addition, for naïve tests beyond the Minimal Standard Model, the number of massless neutrinos, all weak leptonic couplings, or just the axial and/or vector weak leptonic couplings, can be scaled where the scale factor is a fit parameter. These options are not discussed in this paper.

The first processes of interest are the observables which are sensitive to the radiative corrections due to the electroweak interaction without beam polarization, as LEP is currently configured [5, 6]. These include the differential cross sections for the production of $\mu^+\mu^-$, $\tau^+\tau^-$ and e^+e^- final states, the total hadron production cross section, the forward-backward asymmetries of b and c quark production, and the τ polarization. All of these cross sections can be computed with the convolution integral formalism described in the last section. When longitudinally polarized beams become available at LEP, the asymmetries in the polarized cross sections become extremely sensitive tests of the electroweak radiative corrections [1, 2, 30, 38, 41]. The cross sections for production by polarized beams are easily constructed since all of the cross sections are calculated from helicity amplitudes. The differential cross sections for e and μ or τ final states are computed for 100% polarized electron beams on unpolarized positrons for both polarizations. The sum and differences for the total hadronic cross section are also computed so that the individual longitudinal polarization cross sections can be constructed, taking some care with the spin averaging.

As a practical matter, when making fits to data it is important that the computations are done fast, without loss of accuracy. The EXPOSTAR Monte Carlo has been converted to a cross section calculator including the effects of the experimental cuts as described here [3]. The program has been written to take advantage of the vector architecture of the CRAY computer. As the numerical integrations have a fixed structure, they are performed with the use of fixed look-up tables of the flux factors. The calculations of the collision-frame cross sections are performed within vector loops. The result of this is that after initialization, each cross section calculation takes approximately 1 ms. This corresponds to an increase in computational speed by a factor of at least 5×10^4, and in some cases closer to 2.5×10^5, over the Monte Carlo [2, 6] due to the use of rapidity (with its factorization of $H_s(\chi, s)$ as discussed in Sect. 2) to accommodate experimental requirements.

As an example of what can be done with such a program, a study of the sensitivity to variations of the top quark mass was undertaken. In order that the study be conducted to simulate potential data samples, the following procedure was used. A mock data set of cross sections would be calculated for a chosen m_{Higgs}, m_t, M_Z, and N_C. The cross sections were computed at a predefined set of energies and in the case of differential cross sections, at a predefined set of angles. The energies were chosen to correspond to the seven energies of the 1990 LEP resonance scan. To correctly account for the smearing due to the angular dependence of the differential cross sections, the cross sections were evaluated at angles where the cross sections were equal to the average of the differential cross section over equally spaced bins of $\delta \cos\theta' = 0.1$. Hadronic cross sections were computed for $\chi > 0.005$. Leptonic differential cross sections were computed for $|\cos\theta'| < 0.9$, $|Y| < 0.3$, and $\chi > 0.005$, a phase space which is fully sampled by a typical LEP detector. In order to be representative of actual LEP data samples, the numbers of events were calculated with integrated luminosities which closely matched the actual LEP 1990 running conditions (shown in Table 1).

In order to account for the statistical error in luminosity measurement, the cross section that a luminosity detector would be sensitive to, $\sigma_{\mathscr{L}}$, was taken to be representative of a LEP detector as well. Here, $\sigma_{\mathscr{L}} = 26.6$ nb at $\sqrt{s} = M_Z$ and is scaled appropriately by s^{-1} as the energy varies. The expected number of luminosity Bhabha events is then calculated.

A typical LEP experiment has systematic uncertainties associated with its selection efficiencies, backgrounds, and luminosity measurement. For the purpose of this study we assume that the event samples are divided into hadronic events and two leptonic event samples, $\mu + \tau$ and e^+e^- final states. Such a selection avoids the systematic problems associated with separating the τ's from radiative μ events. Bhabha events must be separated out since the physics associated with that process is very different. There

Table 1

Energy (GeV)	88.224	89.220	90.222	91.222	92.216	93.220	94.215
Luminosity (nb)	481	517	448	3638	542	595	640

Table 2

N_{had}	$N_{\mu+\tau}$	$\frac{dN_{\mu+\tau}}{d\cos\theta'}$	$\frac{dN_e}{d\cos\theta'}$	N_{had}^{pol}	$\frac{dN_{\mu+\tau}^{pol}}{d\cos\theta'}$	$\frac{dN_e^{pol}}{d\cos\theta'}$	ΔM_Z	Δm_{top}	ΔN_{col}
X	X						0.010	79	0.029
X		X					0.010	69	0.028
X			X				0.010	97	0.042
X		X	X				0.010	65	0.026
		X	X				0.023	92	0.034
				X			0.010	24	0.033
				X	X		0.010	22	0.023
				X		X	0.010	23	0.027
				X	X	X	0.010	22	0.022
					X	X	0.023	46	0.034

is no t-channel subtraction [42] made, since the EXPOSTAR wide angle $e^+e^-\to e^+e^-$ calculation (Appendices A, B and C) is accurate to better than 0.5% [36] (Appendix B).

To correctly treat the statistical properties of the mock data sample, χ^2 was calculated as

$$\chi^2 = -2\sum_{i,j}\left(N_{ij}^{seen}\ln\left(\frac{N_{ij}^{exp}}{N_{ij}^{seen}}\right) + N_{ij}^{seen} - N_{ij}^{exp}\right),$$

where i denotes the process, j the energy, and $N_{ij}^{exp} = \sigma_i(E_j) * \mathscr{L}_j * \delta_i$ is the theoretically expected number of events computed from the theoretical cross sections ($\sigma_i(E_j)$), the luminosities ($\mathscr{L}_j$), and the systematic coefficients (δ_i). This expression is derived from the Poisson log-likelihood function. For each systematic error parameter δ_i, a term

$$\Delta\chi^2 = \left(\frac{1-\delta_i}{\sigma_{\delta_i}}\right)^2$$

is added to the total χ^2. The minimization is done with MINUIT [37].

In each of the fits, the following physics parameters are fit besides the 3 (or 4) systematic coefficients (δ_i) and the 7 luminosities ($\mathscr{L}_j$): the Z mass (M_Z), the top quark mass (m_t), and the number of colors (N_C). The luminosities and systematic error coefficients are treated as fit parameters in order that a realistic simulation of fit accuracy, including correlations, be obtained. The data was generated with $M_Z = 91.2$ GeV, $m_t = 160$ GeV, and a Higgs mass, $m_{Higgs} = 100$ GeV. A systematic error of 1.34% was assigned to the luminosity measurement, 0.6% was assigned for the hadronic event selection, and 0.5% assigned the leptonic event selection. No systematic error was assigned for the separation of the wide angle Bhabha events from the $\mu+\tau$ sample.

For the polarized beam measurements the luminosity at each point was divided equally between the two polarizations and a beam polarization of 45% was assumed. For these fits a number of events was generated for each polarization and each process considered and twice as many terms were summed in χ^2 in the form described above. For the polarized beam studies, a systematic uncertainty for the fractional error of the polarization of 2.5%, corresponding to an uncertainty of 1.1% in magnitude, was assumed.

The results are shown in Tables 2–4. The errors quoted are the one standard deviation parabolic errors. The true error in m_t is asymmetric and a more careful error analysis would be made for real data. As this procedure is very CPU intensive and we are interested in relative accuracy here, only the symmetric errors were determined. All of the results shown in Tables 2–4 are from converged fits and exactly the input parameters were found.

Table 3

N_{had}	$N_{\mu+\tau}$	$\frac{dN_{\mu+\tau}}{d\cos\theta'}$	$\frac{dN_e}{d\cos\theta'}$	ΔM_Z	Δm_{top}	ΔN_{col}
X	X			0.005	44	0.018
X		X		0.005	36	0.016
X			X	0.005	49	0.021
X		X	X	0.004	33	0.015
		X	X	0.010	45	0.019

N_{had}^{pol}	$\frac{dN_{\mu+\tau}^{pol}}{d\cos\theta'}$	$\frac{dN_e^{pol}}{d\cos\theta'}$	ΔM_Z	Δm_{top}	ΔN_{col}
X	X	X	0.004	14	0.012

Table 4

N_{had}	$N_{\mu+\tau}$	$\frac{dN_{\mu+\tau}}{d\cos\theta'}$	$\frac{dN_e}{d\cos\theta'}$	ΔM_Z	Δm_{top}	ΔN_{col}
X	X			0.002	22	0.010
X		X		0.002	15	0.007
X			X	0.002	18	0.008
X		X	X	0.002	14	0.006
		X	X	0.005	21	0.009

N_{had}^{pol}	$\frac{dN_{\mu+\tau}^{pol}}{d\cos\theta'}$	$\frac{dN_e^{pol}}{d\cos\theta'}$	ΔM_Z	Δm_{top}	ΔN_{col}
X	X	X	0.002	9	0.006

A luminosity increase by a factor of 5 (the expected increase for the 1991 LEP run) would produce Table 3, while an increase in luminosity of 25 (perhaps the sum of the four LEP experiments if the 1991 run is very successful) would give Table 4.

When the total hadronic cross section is used in conjunction with the differential cross section to common leptons ($e+\mu+\tau$) the analyzing power of our data sample is maximized. If the systematic error on the beam polarization is not included, the m_t estimates then have accuracies of 19 GeV, 8 GeV and 4 GeV for $P=45\%$ polarized beams with the three luminosities respectively. In that case, longitudinal beam polarization would allow a more sensitive determination of m_t by a factor ≈ 4 than possible without polarization. When the error $\Delta P=1.1\%$ is included, polarization improves the determination of m_t by factors of 3.0, 2.4 and 1.5 respectively for the three luminosities. Polarization would still provide a distinct advantage but it is already beginning to become systematics limited at luminosities corresponding to those which LEP might achieve by the end of 1991 for a single experiment. This gives an indication of how sensitive the measurements are to this effect. It is, therefore, very important to measure the longitudinal beam polarization to accuracies higher than 1% [38].

The τ polarization has not been used here. Neither the additional information from measurements of the forward backward asymmetry for b quarks, nor the exclusive b quark processes, with their independent m_t information [6, 31, 32], were used here. If the correctness of perturbative QCD is assumed, the information from other independent measurements, e.g., energy–energy correlations or jet multiplicity studies, can be used to constrain the strong coupling constant, α_{strong}, and the errors on m_t could be reduced by approximately 20%. This is because α_{strong} would effectively constrain C_{QCD}, removing the large correlation between the N_C and m_t fit parameters.

When the mock data are generated with a Higgs mass of 100 GeV but fit assuming a mass of 500 GeV, the results shift m_t by $+17$ GeV (for 25 times the 1990 luminosity) with no significant shift in the other fit parameters ($\delta\chi^2=0.1$ for 256 degrees of freedom). When the same test is made (i.e., using hadronic total cross section, $\mu+\tau$ and Bhabha differential cross sections, and the standard luminosities) but with polarized beams the m_t shift is $+22$ GeV, with all other results being the same. The low value of $\delta\chi^2$ is indicative of the fact that the constant radiative corrections due to m_t and m_{Higgs} in the ρ parameter [27] cannot be distinguished for this choice of fit samples.

4 Conclusions

The results show that estimates of m_t could be very precise at the end of LEP running in 1991. Each experiment might expect an ≈ 35 GeV error on m_t, if LEP runs successfully and if the Standard Model is correct. The combined error from LEP could be as good as ≈ 15 GeV. There is an additional ≈ 20 GeV error from m_{Higgs}. A proper combined analysis, however, will depend on the degree of availability of all experimental results, in a form convenient for analysis (e.g., to date no LEP experiment has published results for measured differential cross sections).

If $P=45\%$ polarized beams with error $\Delta P=1.1\%$ were available, the error on m_t would be a factor ≈ 1.5 to 3 (depending on the luminosity) smaller than would be possible without polarization. This begins to become systematics-limited at a luminosity corresponding to what might be achieved at LEP for a single experiment. Beams with higher longitudinal polarization and much smaller ΔP [38] yield a real advantage (factor ≈ 4 smaller error) for indirect determinations of m_t from quantum loop effects on high precision data.

Acknowledgements. We would like to thank W. Atwood, T. Burnett, M. Greco, R. Kleiss, S. Selipsky, J. Thomas and L. Trentadue for many useful and informative discussions. BWL would like to thank J. Ellis and the CERN theory group for their kind hospitality at CERN in 1990. This work was partially supported by D.O.E. contract DE FG0587 ER40319 and NSF contract NSF PHY 8917438.

Appendix A: cross sections

A.1 Helicity cross sections

To excellent approximation, the processes of interest at LEP are scattering and annihilation of massless fermions. Thus, helicity amplitudes and cross sections [30] are the most natural objects on which to base fast numerical calculations such as EXPOSTAR [2, 3]. The only exception, b quark production, requires explicit reduction of phase space due to its non-negligible mass. The cross sections for specific initial and final state helicities can be easily computed in the collision-frame and from these the observable cross sections for polarized or unpolarized beams and/or final states. The corresponding experimental cross sections are easily evaluated in the collision-frame by simply binning the data in $\cos\theta'$. Many computational simplifications are achieved in this way, the most powerful being for the Bhabha cross section. The four helicity cross sections in the collision-frame for s channel processes are (l, r = left, right-handed fermions respectively; the first index denotes the initial state and the second, the final state)

$$\left.\frac{d\sigma_{ll}}{d\cos\theta'}\right|_{s'} \equiv \frac{s'}{16\pi}|A_{ll}(s',t')|^2\frac{u'^2}{s'^2},$$

$$\left.\frac{d\sigma_{rr}}{d\cos\theta'}\right|_{s'} \equiv \frac{s'}{16\pi}|A_{rr}(s',t')|^2\frac{u'^2}{s'^2},$$

$$\left.\frac{d\sigma_{lr}}{d\cos\theta'}\right|_{s'} \equiv \frac{s'}{16\pi}|A_{lr}(s',t')|^2\frac{t'^2}{s'^2},$$

$$\left.\frac{d\sigma_{rl}}{d\cos\theta'}\right|_{s'} \equiv \frac{s'}{16\pi}|A_{rl}(s',t')|^2\frac{t'^2}{s'^2},$$

where the amplitudes are the sum of the photon exchange, the Z exchange and the weak (W-W and Z-Z) box contributions which have an additional angular dependence beyond the overall factor of $(1\pm\cos\theta')^2$. Our helicity convention is that spin and momentum are anti-parallel for massless left-handed fermions. The helicity amplitudes

are more fully described in Appendix D. The collision-frame cross sections are then multiplied by an appropriate overall factor for final state radiation. The effects of the initial state radiation are accommodated by performing the convolution integral described in Sect. 2 on all four of these collision-frame cross sections. Lastly, the residual effects of box diagrams containing at least one photon as well as residual bremsstrahlung processes are added, as discussed in Sect. 2. We will call the cross sections constructed in this way 'observed' as distinct from 'collision-frame'.

A.2 s channel cross sections

The collision frame differential cross sections for μ and τ production by unpolarized beams are then

$$\left.\frac{d\sigma}{d\cos\theta'}\right|_{s'}^{\mu,\tau}=\frac{1}{2}\left(\frac{d\sigma_{ll}^{\mu,\tau}}{d\cos\theta'}+\frac{d\sigma_{rr}^{\mu,\tau}}{d\cos\theta'}+\frac{d\sigma_{rl}^{\mu,\tau}}{d\cos\theta'}+\frac{d\sigma_{lr}^{\mu,\tau}}{d\cos\theta'}\right),$$

where a final state correction of

$$1+\frac{4}{3}Q^2\frac{\alpha_*(0)}{\pi},$$

with Q the electric charge of the outgoing fermion, applied. The observed cross sections are then computed as described.

The total hadronic cross section is constructed by replacing the expressions for polarized muon cross sections by like expressions with appropriate $SU(2)\times U(1)$ quantum numbers for the five quark flavors. The total cross section is calculated by integrating each of the polarized quark cross sections over $\cos\theta'$ and then summing them. The delicate integration of the $\cos\theta'$ dependence of the box contributions is discussed in Appendix C.

An additional final state correction for QCD effects multiplies the collision-frame cross sections in the convolution integral. C_{QCD} corresponds to a QCD final state correction due to a measured value of α_{strong}, which if calculated to second order in perturbative QCD would be

$$3\left(1+\frac{\alpha_{strong}}{\pi}+\sqrt{2}\left(\frac{\alpha_{strong}}{\pi}\right)^2\right).$$

Internally the program uses

$$C_{QCD}=N_C\left(1+\frac{\alpha_{strong}^{EXPOSTAR}(q^2)}{\pi}\right),$$

where the number of colors, N_C, is a fit parameter and the running two-loop $\alpha_{strong}^{EXPOSTAR}(q^2)$ is calculated within the program, $\alpha_{strong}^{EXPOSTAR}(-M_Z^2)=0.1253$. Thus a variation in N_C corresponds to a variation in the QCD final state correction. For example, an average value of $\alpha_{strong}=0.115\pm0.010$ has been measured by the LEP experiments from hadronic shape parameters [43]. This measured α_{strong} corresponds to $N_C=2.998\pm0.010$.

A.3 Wide-angle Bhabha (e^+e^-) cross section

The collision-frame Bhabha cross sections are obtained from the s-channel muon calculation through a Fierz transformation [30]

$$\left.\frac{d\sigma_l}{d\cos\theta'}\right|_{s'}^{e^+e^-}=\frac{s'}{16\pi}\left(|A_{ll}(s',t')+A_{ll}(t',s')|^2\frac{u'^2}{s'^2}+|A_{lr}(s',t')|^2\frac{t'^2}{s'^2}+|A_{lr}(t',s')|^2\right),$$

and

$$\left.\frac{d\sigma_r}{d\cos\theta'}\right|_{s'}^{e^+e^-}=\frac{s'}{16\pi}\left(|A_{rr}(s',t')+A_{rr}(t',s')|^2\frac{u'^2}{s'^2}+|A_{rl}(s',t')|^2\frac{t'^2}{s'^2}+|A_{rl}(t',s')|^2\right).$$

All $*$ running couplings are evaluated at $q^2=-s'$ or $q^2=-t'$ (Euclidean metric) as appropriate and the helicity amplitudes are as defined for the muon cross section (see Appendix D), evaluated at the appropriate momenta-squared: (s',t') for s channel and (t',s') for t channel. This, of course, reflects only the crossing symmetry of the electroweak theory. Thus, the f^{WW} and f^{ZZ} functions contained in the amplitudes again represent the contribution from the heavy weak boxes for either s or t channel. The weak vertex parts and the $*$ running coupling are written as analytic functions of q^2, and so continue to the spacelike region. The imaginary parts of the quantum-loop vector self-energy parts $\Pi(q^2)$ (as well as weak vertex and heavy box parts) vanish for space-like momentum transfers so the widths don't appear in the t channel amplitudes. (The heavy box 'left-hand cut' is not included in EXPOSTAR.). In this manner the collision-frame Bhabha cross section can be constructed to the same accuracy (1-loop plus certain higher-order improvements) as the s-channel processes.

The use of two different flux factors for s and t channel (see Sect. 2 and Appendix B respectively) ensures that exponentiated soft and collinear radiation effects are not overcounted $(i,j=l,r)$.

$$A_{ij}(s',t')\to\sqrt{H_s(\chi,s)}\,A_{ij}(s',t'),$$

$$A_{ij}(t',s')\to\sqrt{H_t(\chi,s)}\,A_{ij}(t',s').$$

The resulting cross sections are correct for exponentiated radiation [7], and leading logs to α^4, in pure s and t channel processes and the cross terms agree with [14]. In addition the non-collinear terms to order α^3 are correct for all three components [14], and the next to leading and non-collinear terms for the s channel to order α^4 are included as before [9]. After the convolutions, the remaining order α^3 corrections must be added. The terms $\square_{Z\gamma}$ and $\square_{\gamma\gamma}$ added to the convolution integrals are as for the other leptons, but now the t and s-t bremsstrahlung cross terms along with the appropriate t channel boxes with at least one photon must also be computed and included along with appropriate final state radiation factors. Care is taken to exclude those parts already included in flux factors so as not to overcount one-loop effects.

Thus, a complete one-loop QED and electroweak calculation [6], supplemented by certain higher-order electroweak effects and exponentiation of soft and collinear (and most of the non-collinear) radiation [14, 36], is done

for Bhabha scattering in the collinear radiation approximation in EXPOSTAR.

A.4 b and c quark forward backward asymmetries

The quark forward-backward asymmetries are constructed from ratios of sums and differences of polarized cross sections. It is convenient to define the two collision frame cross sections:

$$\left.\frac{d\sigma^{dif}_{quark}}{d\cos\theta'}\right|^{b,c}_{s'} = \frac{d\sigma^{b,c}_{ll}}{d\cos\theta'} + \frac{d\sigma^{b,c}_{rr}}{d\cos\theta'} - \frac{d\sigma^{b,c}_{lr}}{d\cos\theta'} - \frac{d\sigma^{b,c}_{rl}}{d\cos\theta'},$$

and

$$\left.\frac{d\sigma^{tot}_{quark}}{d\cos\theta'}\right|^{b,c}_{s'} = \frac{d\sigma^{b,c}_{ll}}{d\cos\theta'} + \frac{d\sigma^{b,c}_{rr}}{d\cos\theta'} + \frac{d\sigma^{b,c}_{lr}}{d\cos\theta'} + \frac{d\sigma^{b,c}_{rl}}{d\cos\theta'},$$

because of their angular integration properties. The QCD and QED final state corrections are only applied to the total cross section. The angular integration to the detector limit is performed analytically for the overall angular factor, with the weak box contributions integrated numerically at initialization. Next, the convolution over initial state radiation is done and the appropriate effects of boxes (integrated over angles) with at least one photon and residual bremsstrahlung effects added to get the observed cross sections. The ratio of these observed cross sections is the forward-backward asymmetry.

$$A_{quark}(b,c) = \frac{\sigma^{dif}_{quark}(b,c)}{\sigma^{tot}_{quark}(b,c)}.$$

The reduction of b quark final phase space due to its non-zero mass is taken into account with factors of $\beta \equiv \sqrt{1-4m_b^2/s'}$.

A.5 τ polarization asymmetry

The τ polarization asymmetry is most easily written in terms of final state collision-frame helicity cross sections.

$$\left.\frac{d\sigma^{\tau}_{r}}{d\cos\theta'}\right|_{s',\cos\theta'} = \frac{d\sigma^{\tau}_{rr}}{d\cos\theta'} + \frac{d\sigma^{\tau}_{lr}}{d\cos\theta'},$$

$$\left.\frac{d\sigma^{\tau}_{l}}{d\cos\theta'}\right|_{s',\cos\theta'} = \frac{d\sigma^{\tau}_{ll}}{d\cos\theta'} + \frac{d\sigma^{\tau}_{rl}}{d\cos\theta'},$$

using the differential cross sections described above. The polarization asymmetry as a function of s and $\cos\theta'$ is then computed from the observed cross sections as

$$P_{\tau} = \frac{d\sigma^{\tau}_{l}/d\cos\theta' - d\sigma^{\tau}_{r}/d\cos\theta'}{d\sigma^{\tau}_{l}/d\cos\theta' + d\sigma^{\tau}_{r}/d\cos\theta'},$$

where 'observed' means after convolution with initial state radiation, inclusion of final state radiation factors, boxes with at least one photon and residual bremsstrahlung effects. No provision for τ decay [5, 6] is made in EXPOSTAR. In the current scheme the polarized differential cross sections are evaluated. The total polarization integrated over a symmetric angular range can be evaluated numerically by summing the differential polarizations at judiciously chosen angles (as described in the mock data section). It should be noted that the polarization is only significant in the forward hemisphere. The backward hemisphere adding an almost entirely unpolarized cross section and thereby decreasing the sensitivity of this process to interesting electroweak loop effects.

A.6 Beam polarization cross sections

The expressions for processes involving initial beam longitudinal polarization are particularly obvious in the helicity cross section and helicity amplitude formalism used by EXPOSTAR for massless external fermions in four-fermion processes. We may then form total or differential cross sections with which to fit data. The best known test of electroweak radiative corrections is the beam polarization asymmetry A_{LR} in $e^+e^- \to$ hadrons [30, 38, 41, 44] formed from the ratio of the difference over the sum of total cross sections to hadrons with left-handed and right-handed beams. In our mock-data fit, we also use polarized differential cross sections to leptons.

Appendix B: t-channel calculation

The t-channel flux factor and structure functions are written in the second form of Nicrosini and Trentadue [9], with the appropriate non-collinear terms for the t-channel [14].

$$H_t(\chi, s) = \Delta_t(\beta+\beta_{int})(1-\chi)^{\beta+\beta_{int}-1} - \beta_t(1+\chi)/2 + \frac{\beta_t^2}{8}[(1+\chi)(3\ln(\chi) - 4\ln(1-\chi)) - (4/(1-\chi))\ln(\chi) - (5+\chi)],$$

$$\beta = \frac{2\alpha}{\pi}\ln\left(\frac{s}{m^2}-1\right),$$

$$\beta_t = \frac{2\alpha}{\pi}\left[\ln\left(\frac{s}{m^2}\right) + \ln\left(\frac{1-\cos\theta}{2}\right) - 1\right] = \frac{2\alpha}{\pi}\ln\left(\frac{|t|}{m^2}-1\right),$$

$$\beta_{int} = \frac{4\alpha}{\pi}\ln\left(\frac{u}{t}\right),$$

$$\Delta_t = 1 + \frac{\alpha}{\pi}\left[\frac{3}{2}\ln\left(\frac{|t|}{m^2}-1\right) - \frac{\pi^2}{6} - \frac{1}{2} - \ln^2\left(\frac{1-\cos\theta}{2}\right)\right] + \left(\frac{\alpha}{\pi}\right)^2\left(\frac{9}{8} - \frac{\pi^2}{3}\right)\ln^2\left(\frac{|t|}{m^2}-1\right).$$

The electron structure functions needed to correct for the rapidity cut can be constructed from the above terms,

as in [9].

$$D_t(x,s)=\Delta_t'\frac{(\beta+\beta_{\rm int})}{2}(1-x)^{(\beta+\beta_{\rm int})/2-1}-(1+x)\beta_t/4$$
$$+(\beta_t^2/32)((1+x)(3\ln x-4\ln(1-x))$$
$$-4\ln x/(1-x)-5-x),$$

where $\Delta_t'^2=\Delta_t^2+\beta_t^2\pi^2/24$. The terms proportional to β_t and β_t^2 cancel the leading logs from $\int H_t(\chi,s)\mathrm{d}\chi=k$, k being the finite remainder due to the non-collinear terms. The initial-final state interference term, $\beta_{\rm int}$, makes a negligible ($\leq 10^{-3}$) contribution to the results when $|\cos\theta'|<0.9$ and a rapidity cut, $|Y|<0.3$, is applied to a pure t-channel cross section (e.g. $e\mu$ scattering). Without a Y cut, the difference over the same angular range can be as large as 8%. The s-channel process is also insensitive to the initial-final state factorizable term. The s-t interference in the vicinity of the Z pole is more sensitive due to its strong energy dependence, and the inclusion of $\beta_{\rm int}$ contributes a maximum of 3×10^{-3} to the integrated wide-angle Bhabha cross section at M_Z-1 GeV.

The t-channel calculation of the EXPOSTAR and ALIBABA [15] programs have been compared and found to be in agreement to at least 0.5%. The comparison is non-trivial due to the different cuts used by the two programs. ALIBABA cuts in the observed variables of the final state leptons: momentum, lab angle and polar acollinearity. EXPOSTAR cuts in the collision-frame variables: rapidity, invariant energy, and scattering angle. A comparison between the two requires the use of a Monte Carlo event generator where both sets of cuts can be applied to a common event sample. The Born term is of order α^2. The best wide angle event generator available is BHABMC [18], but it only calculates to order α^3 without exponentiation. The two semi-analytic Bhabha calculations include order α^3 and important terms of order α^4 with exponentiation. Hence, a rigorous comparison is not possible, but limits can be determined.

If BHABMC is run in the t-channel only, the ratio R of the number of events passing the ALIBABA cuts ($P_{\rm min}>1$ GeV, $|\cos\theta_{\rm lab}|<0.9$, acol$<25°$) to the number of events passing the EXPOSTAR cuts ($|Y|<0.3$, $\chi>0.005$, $|\cos\theta'|<0.9$) is found to be 0.945. The deviation of this ratio from 1 is due just to radiative corrections. If this deviation is assumed to be fully correlated to the cross section, then an upper limit of the value of R that would be found for an order α^4, exponential calculation can be approximated from the relation

$$\frac{1-R_{\alpha^4,\,\rm exponentiated}}{1-R_{\alpha^3,\,\rm unexponentiated}}\approx\frac{\sigma_{\rm born}-\sigma_{\alpha^4,\,\rm exponentiated}}{\sigma_{\rm born}-\sigma_{\alpha^3,\,\rm unexponentiated}}.$$

The right-hand side can be computed using the ALIBABA program, as it has as an option the capability to compute to order α^3, unexponentiated. Since both ALIBABA and EXPOSTAR find $\sigma_{\rm born}=556.6$ pb (for $M_Z=91.17$, $m_{\rm Higgs}=100$, $m_t=120$, and $\sqrt{s}=91.2$) within the cuts, the relation implies $R_{\alpha^4,\,\rm exponentiated}<0.956$. With the order α^3 ratio from the BHABMC results, the range of $R_{\alpha^4,\,\rm exponentiated}$ is given by

$$0.945<R_{\alpha^4,\,\rm exponentiated}<0.956.$$

The observed ratio of the two calculations for the two sets of cuts is 0.949. The pure t-channel contribution to the full Bhabha cross section is about 1/3 of the total at the Z pole, over the angular range stated above. The accuracy of the s-channel calculation has long been established [6], and since the cross term is obtained by squaring the amplitudes, the uncertainties stated here and in Sect. 2 lead to a conservative estimate for the accuracy of 0.5%.

Appendix C: Box diagram calculations

The QED box and bremsstrahlung contributions are calculated from analytic expressions allowing the same expressions to be used for both s- and t-channel processes. The Z-γ box expression is due to Brown, Decker, and Paschos [39] to which the appropriate bremsstrahlung contribution has been added to account for the additional finite terms and to cancel the photon mass cutoff. In the same notation of [39], a corresponding analytic expression for the $\gamma\gamma$ boxes is ($s+t+u=0$)

$$f_{\gamma\gamma}(s,t,u)=\frac{1}{u}\left[\ln\left(\frac{-t}{\lambda^2}-i\varepsilon\right)-\ln\left(\frac{-s}{\lambda^2}-i\varepsilon\right)\right]$$
$$+\frac{t-u}{u^2}\left\{\frac{\pi^2}{2}+\frac{1}{2}\left[\ln\left(\frac{-s}{\lambda^2}-i\varepsilon\right)\right.\right.$$
$$\left.-\ln\left(\frac{-t}{\lambda^2}-i\varepsilon\right)\right]^2+\left[\ln\left(\frac{-s}{\lambda^2}-i\varepsilon\right)$$
$$\left.\left.-\ln\left(\frac{-s}{\lambda^2}+i\varepsilon\right)\right]\left[\ln\left(\frac{-t}{\lambda^2}-i\varepsilon\right)-\ln\left(\frac{-t}{\lambda^2}+i\varepsilon\right)\right]\right\}$$
$$+\frac{2}{s}\left\{\ln\left(\frac{-s}{\lambda^2}+i\varepsilon\right)\left[\ln\left(\frac{-t}{\lambda^2}-i\varepsilon\right)\right.\right.$$
$$\left.-\ln\left(\frac{-u}{\lambda^2}-i\varepsilon\right)\right]+\left[\ln\left(\frac{-s}{\lambda^2}-i\varepsilon\right)$$
$$-\ln\left(\frac{-s}{\lambda^2}+i\varepsilon\right)\left]\left[\ln\left(\frac{-t}{\lambda^2}+i\varepsilon\right)\right.\right.$$
$$\left.\left.-\ln\left(\frac{-u}{\lambda^2}+i\varepsilon\right)\right]\right\},$$

and is independent of the photon mass cutoff λ when added to soft bremsstrahlung contributions. This gives the same cross section contribution for the s-channel found by Böhm and Hollik [40].

Calculation of the total hadronic cross section is complicated by the angular dependences of the f^{WW}, f^{ZZ}, $\square_{Z\gamma}$, and $\square_{\gamma\gamma}$ terms. The $\square_{Z\gamma}$ and $\square_{\gamma\gamma}$ terms are integrated over $\cos\theta'$ numerically. For the b and c quark cross sections discussed in Appendix A, the integrations are over a user defined symmetric range. For the hadronic total cross sections the integration is over all $\cos\theta'$. The f^{WW} and f^{ZZ} amplitudes, included in the helicity amplitudes and discussed in Appendix D, are integrated in a like manner over $\cos\theta'$ with an additional weight of $\frac{3}{8}(1\pm\cos\theta')^2$. This produces the correct cross terms in the integrated matrix element. These integrations are done once at initialization for all of the energies specified.

Appendix D: Helicity amplitudes

We use the Euclidean metric (with timelike squared momenta negative) throughout this section and begin by collecting some formulae from the literature: The $SU(2)\times U(1)$ helicity matrix elements for neutral and charged current four-fermion processes for massless external fermions are $\mathcal{M}^{NC}$ and $\mathcal{M}^{CC}$, found respectively in (A.38) and (A.39) in [1]. Here, (Q, I_3, I_+, I_-, I^2) are respectively the electric charge, third component of isospin, raising operator and lowering operator for isospin and isospin-squared ($I^2=I(I+1)$) for one of the fermions and, of course, $(Q', I'_3, I'_+, I'_-, I'^2)$ are the same quantities for the other fermion. Left-handed (l) and right-handed (r) fermions are regarded as distinct species and the helicity, preserved along the fermion line, is always associated with the *particle*. Here we focus on the matrix elements for neutral current processes and give the following examples to illustrate our notation: i) left-handed electron e_l scattering from right-handed anti-electron $\bar{e}_l$ in the t channel

$$\mathcal{M}^{NC}_{ll}(e_l\bar{e}_l\to e_l\bar{e}_l;\ q^2=-t)$$
$$=\mathcal{M}^{NC}(Q=-1,\ I_3=-\tfrac{1}{2};\ Q'=-1,\ I'_3=-\tfrac{1}{2};\ q^2=-t)$$

ii) left-handed electron e_l and right-handed anti-electron $\bar{e}_l$ annihilating to right-handed electron e_r and left-handed anti-electron $\bar{e}_r$ in the s channel

$$\mathcal{M}^{NC}_{lr}(e_l\bar{e}_l\to e_r\bar{e}_r;\ q^2=-s)$$
$$=\mathcal{M}^{NC}(Q=-1,\ I_3=-\tfrac{1}{2};\ Q'=-1,\ I'_3=0;\ q^2=-s)$$

iii) right-handed electron e_r and left-handed anti-electron $\bar{e}_r$ annihilating to left-handed u quark u_l and right-handed u anti-quark $\bar{u}_l$ in the s channel

$$\mathcal{M}^{NC}_{rl}(e_r\bar{e}_r\to\bar{u}_lu_l;\ q^2=-s)$$
$$=\mathcal{M}^{NC}(Q=-1,\ I_3=0;\ Q'=\tfrac{2}{3},\ I'_3=+\tfrac{1}{2};\ q^2=-s).$$

All other neutral current matrix elements follow by simply substituting the appropriate quantum numbers (for flavors and helicities) and evaluating at the appropriate q^2.

In order to write the residual weak vertex parts [1, 6, 45] not contained in the $*$ running couplings we will need the three functions ρ, Λ, and Ξ in (2.7), (2.8) and (2.9) of [32]. The third argument of these functions m_i^2 is the mass-squared of the fermion *internal* to the weak vertex part. It is zero for all but b quark production. In that case $m_i=m_t$ since the top quark appears in graphs with internal W's. Define $\rho_W=\rho(q^2, M_W^2, m_i^2)$, $\rho_Z=\rho(q^2, M_Z^2, 0)$, $V^\Xi=e_*^2\Xi(q^2, M_W^2, m_i^2)/(16\pi^2 s_*^2)$, $\Lambda_W=\Lambda(q^2, M_W^2, m_i^2)$ as well as $\Gamma'(q^2)$ from (B.16) in [1]. We will need the auxiliary functions

$$V^{nab}=\frac{e_*^2}{16\pi^2 s_*^2}(-\rho_W-\Lambda_W-16\pi^2(\Gamma'-\Gamma'(0))),$$

$$V=\frac{e_*^2}{16\pi^2 s_*^2}\left(\frac{1}{2}\rho_W+\left(\frac{I_3-s_*^2Q}{c_*}\right)^2\rho_Z\right),$$

$$V'=\frac{e_*^2}{16\pi^2 s_*^2}\left(\frac{1}{2}\rho_W+\left(\frac{I'_3-s_*^2Q'}{c_*}\right)^2\rho_Z\right).$$

Now make the substitutions in $\mathcal{M}^{NC}$:

$$I_3\to I_3(1+V)+I_3V^{nab},$$
$$Q\to Q(1+V)+I_3V^{nab},$$
$$I'_3\to I'_3(1+V')+I'_3V^{nab},$$
$$Q'\to Q'(1+V')+I'_3V^{nab},$$

evaluating the quantum numbers appropriately for different fermion species (flavors and helicities). Finally, we make the additional substitution

$$I_3\to I_3(1+V^\Xi),$$
$$I'_3\to I'_3(1+V^\Xi),$$

only in the Z-exchange term of $\mathcal{M}^{NC}$ (and throw away terms with products of more than 2 vertex parts) in order to include all one-loop weak vertex parts. Such substitutions are made in both the real and various imaginary parts of $\mathcal{M}^{NC}$ (e.g. in the 's-dependent width' Γ_Z^* introduced in (C.10) of [1]) in order to ensure their proper influence on physical observables (e.g. the on-resonance cross section is approximately the ratio of products of widths). We will call the neutral current helicity matrix elements, constructed in this way so as to contain the weak vertices, $\tilde{\mathcal{M}}^{NC}(q^2)$ [1, 2].

The weak boxes [6, 45] with two internal heavy gauge bosons can be written in a surprisingly simple form using the algebraic reduction techniques in [46]. We take the expression for the crossed W-W box diagram with final state b quarks, including the effect of a heavy top quark, from [32] and focus on the function $I(s, u, M_W^2, m_t^2)$ in (3.1) there. Now define two new functions

$$\Theta_{cross}(s, t, M^2, m^2)$$
$$=\frac{1}{4\pi^2}I(s, -s-t, M^2, m^2),$$

$$\Theta_{uncross}(s, t, M^2)$$
$$=\frac{1}{4\pi^2}\{C_0(0, -s, 0; 0, M^2, M^2)$$
$$-\frac{(s+t)}{2}D_0(0, -s, 0, s+t, 0, 0; 0, M^2, M^2, 0)\},$$

with the notation of [46]. The boxes with two internal W's are easily written

$$f^{WW}(s, t)=\left(\frac{e_*}{\sqrt{2s_*}}\right)^4\{2((I^2-I_3^2)(I'^2-I_3'^2)-I_3I'_3)$$
$$\times\Theta_{uncross}(s, t, M_W^2)+2((I^2-I_3^2)(I'^2-I_3'^2)$$
$$+I_3I'_3)\Theta_{cross}(s, t, M_W^2, m_i^2)\}.$$

From this equation we see that f_{ij}^{WW} vanishes for all helicities except $i=j=l$. For doublet-doublet scattering, one of the crossed or uncrossed W-W box diagrams vanishes. Further, $m_i^2=0$ except for b quarks where $m_i^2=m_t^2$. The boxes with two internal Z's give

$$f^{ZZ}(s, t)=\left(\frac{e_*}{s_*c_*}\right)^4((I_3-Qs_*^2)^2(I'_3-Q's_*^2)^2)$$
$$\times(\Theta_{uncross}(s, t, M_Z^2, 0)+\Theta_{cross}(s, t, M_Z^2, 0)).$$

The s channel helicity amplitudes used in EXPOSTAR are then

$$A_{ij}(s,t) = -\tilde{\mathcal{M}}_{ij}^{\mathrm{NC}}(q^2=-s) + f_{ij}^{WW}(s,t) + f_{ij}^{ZZ}(s,t),$$

where, as usual, the various quantum numbers are evaluated for a given flavor and helicity. The Feynman rules used to derive this amplitude can be found in [47], the first MSM one-loop electroweak calculations of $e^+e^- \to \mu^+\mu^-$ near the Z, in which much of the modern one-loop technology is introduced. The amplitudes include all one loop electroweak corrections as well as certain higher order improvements discussed in Sect. 3. Electroweak crossing symmetry can be used to write these in the t channel by simply intechanging $s \leftrightarrow t$.

References

1. D.C. Kennedy, B.W. Lynn: SLAC-PUB 4039 (July 1987); D.C. Kennedy, B.W. Lynn: Nucl. Phys. B322 (1989) 1
2. D.C. Kennedy, B.W. Lynn, C.J.-C. Im, R.G. Stuart: Nucl. Phys. 321B (1989) 83
3. EXPOSTAR 1990, D.C. Kennedy, D. Levinthal, B.W. Lynn, R.G. Stuart: VXCERN:: DISK$ALEPH1: [LEVINTHAL. EXPOSTAR], equivalent to 22718::22DUS304:[LEVINTHAL.EXPOSTAR]
4. S. Glashow: Nucl. Phys. 22 (1961) 579; S. Weinberg: Phys. Rev. Lett. 19 (1967) 1264; A. Salam: in: Elementary particle physics, N. Svartholm (ed.) p. 367. Stockholm: Almqvist and Wiksell Sweden (1968)
5. Physics at LEP. J. Ellis, R. Peccei (eds.), CERN Report 86-02, 1986 and references therein
6. Physics at LEP. G. Altarelli et al. (eds.), CERN Report 89-08, 1989 and references therein
7. D.R. Yennie, S.C. Frautschi, H. Surra: Ann. Phys. 13 (1961) 379
8. E.A. Kuraev, V.S. Fadin: Sov. J. Nucl. Phys. 41 (1985) 466
9. O. Nicrosini, L. Trentadue: Phys. Lett. B196 (1987) 551
10. F.A. Berends, W.L. Van Neerven, G.J.H. Burgers: Nucl. Phys. B297 (1988) 429
11. S. Drell, C.N. Yan: Phys. Rev. Lett. 25 (1970) 316
12. A.L.S. Angelis et al.: Nucl. Phys. B209 (1982) 284; D. Levinthal: Ph.D. thesis Nevis Report 234 Columbia Univ. (1980)
13. S. Jadach, Z. Was: Phys. Rev. D41 (1990) 1425
14. M. Greco: Riv. Nuovo Cimento N5 Vol. 11 (1988)
15. W. Beenakker, F.A. Berends, S.C. Van der Marck: Nucl. Phys. B349 (1991) 323
16. J.A.M. Vermaseren: Proceedings International Workshop on Gamma Gamma Interactions, Amiens April 1980. Berlin, Heidelberg, New York: Springer
17. S. Jadach, Z. Was: Phys. Lett. B219 (1989) 103
18. F.A. Berends, R. Kleiss, W. Hollik: Nucl. Phys. B304 (1988) 712
19. R. Kleiss: Ph.D. thesis, University of Leiden (1982)
20. S. Willenbrock, G. Valencia: Phys. Lett. B259 (1991) 373
21. R.G. Stuart: Phys. Lett. B262 (1991) 113
22. H. Georgi, H. Quinn, S. Weinberg: Phys. Rev. Lett. 33 (1974) 451
23. M. Consoli, W. Hollik, F. Jegerlehner: in [6]; G. Gounaris, D. Schildknecht: Z. Phys. C – Particles and Fields 40 (1988) 447; M. Kuroda, G. Moultaka, D. Schildknecht, Nucl. Phys. B350 (1991) 25
24. B.W. Lynn: SLAC-PUB 5077, SU-ITP-867, August 1989, first introduced the generally gauge invariant Π^* combinations of one loop vector self-energies and non-abelian parts of weak vertices and boxes. In the subset of 't Hooft-Feynman R_ξ gauges these were shown, by explicit calculation, to be independent of the gauge parameter ξ by Kuroda, Moultaka and Schildknecht, see [23]. The $*$ scheme [1] simply defines certain functions $g(s,t)$ (chosen to be small in magnitude for all low energy four fermion scattering processes) and absorbs $\Pi^* + g$ into running couplings. The convenient but otherwise arbitrary g's force (among other things) the $*$ couplings to run with the proper UV renormalization group β functions [22] at large q^2. The g's are explicitly subtracted out in helicity matrix elements; to one loop, this procedure is equivalent to adding zero to the bare Lagrangian
25. B.W. Lynn, S.B. Selipsky, R.G. Stuart, D. Levinthal: Boston University preprint, BUHEP-90-36, 1991
26. J. Van der Bij, M. Veltman: Nucl. Phys. B231 (1984) 205
27. M. Veltman: Nucl. Phys. B123 (1977) 89; M. Einhorn, D. Jones, M. Veltman: Nucl. Phys. B191 (1981) 146
28. A. Djouadi, C. Verzegnassi: Phys. Lett. B195 (1987) 265; A. Djouadi: Nuovo Cimento A100 (1988) 357
29. H. Burkhardt, F. Jegerlehner, G. Penso, C. Verzegnassi: in: Proceedings of [38]
30. B.W. Lynn, M.E. Peskin, R.G. Stuart: in: Physics at LEP, J. Ellis, R. Peccei (eds.), CERN Report 86-02 Vol 1 (1986) 90
31. M. Böhm, W. Hollik, H. Speisberger: Fortschr. Phys. 34 (1986) 687; A.A. Akhundov, D.Yu. Bardin, T. Riemann: Nucl. Phys. B276 (1988) 1
32. B.W. Lynn, R.G. Stuart, Phys. Lett. B252 (1990) 676
33. B.W. Lynn, SLAC Pub. 3358, 1984; J. Ellis, J. Rudaz, N.D. Tracas; Phys. Lett. B192 (1987) 453
34. M.E. Peskin, T. Takeuchi: Phys. Rev. Lett. 65 (1990) 964; M. Golden, L. Randall; FERMILAB-PUB-90/83-T; B. Holdom, J. Terning: Phys. Lett. B247 (1990) 88; A. Dobado, D. Espiru, M.J. Herrero: Phys. Lett. B255 (1991) 405; R.N. Cahn, M. Suzuki: LBL Berkeley preprint 30351 (1991); for the effects of technicolor loops on non-LEP physics see: S. Chadra, M.E. Peskin: Nucl. Phys. B185 (1981) 61; B187 (1981) 541
35. M.E. Peskin, T. Takeuchi: in [34]; G. Altarelli, R. Barbieri: Phys. Lett. B253 (1991) 161; D.C. Kennedy, P. Langacker: University of Pennsylvania preprint UPR-0436T (1990); B. Grinstein, M. Wise: Harvard Caltech preprint, HUTP-91/A015, CALT-68-1720 (1991) have recently gone beyond these papers and consider certain non-renormalizable operators; these were also previously classified in [1]
36. S. Jadach, E. Richter-Was, B.F.L. Ward, Z. Was: preprint CERN-TH.5995/91, UTHEP-91-02-01
37. F. James, M. Roos: CERN Report D506 (1989)
38. Polarization at LEP: G. Alexander et al. (eds.), CERN Report 88-06 1988 and references therein
39. R.W. Brown, R. Decker, E.A. Paschos; Phys. Rev. Lett. 52 (1984) 1192
40. M. Böhm, W. Hollik: Nucl. Phys. B204 (1982) 45
41. B.W. Lynn, R.G. Stuart: Nucl. Phys. B253 (1985) 216
42. ALEPH preprint, CERN.PRE/90-104 (1990), p. 26, Table 4, Fig. 12
43. M. Schmelling: 1991 Aspen Winter Conference on Elementary Particle Physics (1991) Aspen
44. B.W. Lynn, C. Verzegnassi: Phys. Rev. D35 (1987) 3326
45. R.G. Stuart: Oxford University D. Phil. thesis, Rutherford Appleton Laboratory Report RAL T008 (1985)
46. R.G. Stuart: Comput. Phys. Commun. 48 (1988) 367; R.G. Stuart, A. Góngora-T: Comput. Phys. Commun. 56 (1990) 337
47. G. Passarino, M. Veltman: Nucl. Phys. B160 (1979) 151; M. Consoli: Nucl. Phys. B160 (1979) 208